EFFECTS OF ISOTHERMAL OXIDATION ON THE LOCAL WEAR BEHAVIOUR OF LASER CLADDED INCONEL 625 COATINGS

D. Verdi[1](*), M. A. Garrido[1] , C. Múnez[1], P. Poza[1]
[1] DIMME – Durabilidad e Integridad Mecánica de Materiales Estructurales. Escuela Superior de Ciencias Experimentales y Tecnología. Universidad Rey Juan Carlos. c/Tulipán s/n, Móstoles, Madrid, Spain. (*) davide.verdi@urjc.es.

ABSTRACT
Ni-based alloys, such as Inconel superalloys, are characterized by high strength, excellent fabricability (including joining), and outstanding corrosion resistance. However, their use is limited by their high cost. Ni-based coatings are used on carbon steel components in order to increase their service life under extreme conditions. Laser cladding deposition has emerged as an excellent method for processing Ni-based coatings. In this work, the evolution of the local wear behaviour of Inconel 625 laser cladded coatings after high temperature isothermal oxidation treatments have been investigated.
KEYWORDS: Inconel 625, high temperature isothermal oxidation, depth sensing indentation (DSI), local scratch tests, wear micromechanisms.

1.- INTRODUCTION
Inconel 625 is a Ni-base superalloy constituted by an austenitic Ni-Cr matrix, with other elements like Mo and Nb that generate an alloy with a high resistance to corrosion environments, oxidation and carburization [1]. This characteristics permit its practical use from cryogenic to about 950 *ºC*, in different industrials sectors like aerospace, chemical, petrochemical, marine, nuclear, and power generation among others [2-4].
The main disadvantage of this alloy compared with the most common stainless steels, is its price. Its application as superficial coating permits to reduce these costs increasing the component performance [5,6].
Thermal sprays techniques are the common methods used to obtain Inconel 625 coatings. Among them, High-Velocity Oxy-Fuel (HVOF) and Plasma Spraying (PS) techniques are the most traditional and well known. The main problem correlated with the thermal spraying methods is the deterioration of the substrate properties subjected to high processing temperatures for large periods. In the last two decades, the development of new high power lasers, permits to explore new coatings techniques, like the laser cladding [4,6,7].
Laser cladding is a welding method where the coating, also known as “clad”, is formed by melting a filler material, in form of powder or wire, by means of a laser beam. The energy supplied is also used to melt a small amount of substrate. In this way, a strong metallurgical bond between clad and substrate is achieved. The coatings could be processed in two or one step. In the first case, the added material is pre-placed on the substrate before to be treated by the laser. In the second case, the filler is directly injected in the laser beam.
Inconel 625 was demonstrated to be processed by one step laser cladding [4,7,8].

In addition to a better adhesion, laser cladding provides coatings with higher properties than those obtained by thermal spray. Clads free of pores and cracks were realised. In addition, a reduced heat-affected zone (HAZ) is produced in the substrate [9,10].
Due to its applications, such as turbines rotor parts in aircraft engines or for energy production, these coatings could be subjected to local damages derived from the impact with hard particles becoming from the extern or generated into the system, like oxide particles formed at high temperature. The behaviour of the material against the action of a hard asperity could be studied by means of local scratch tests, that permits to avoid the synergism effects of the multiple passes and the contribution of multiple asperities obtained in a conventional macroscopic wear test.
The microstructure, the mechanical properties, and the local wear behaviour of laser cladded Inconel 625 coatings were presented in previous works [11,12] but, at the authors' knowledge, no studies about the evolution at high temperature of the local wear micromechanisms were done at the moment. In this research, the effects of the exposition at isothermal high temperature oxidation conditions on the local wear behaviour of Inconel 625 clads were studied. The relationship between the microstructure and the mechanical properties and its evolution with temperature were investigated.

2.- MATERIAL AND METHODS

Inconel 625 alloy was deposited onto previously sandblasted 316L stainless steel (ASTM A276) coupons, with dimensions 50 *mm* x 30 *mm* x 5 *mm* (length x width x thickness).
A Rofin-Dilas High-Power Diode Laser (HPDL), with a wavelength of 940 *nm* and a maximum output power of 1300 *W* was used. Inconel 625 powder was directly fed into a coaxial projection head mounted on the laser equipment. Argon was used as protective and powder carrier gas.
The Inconel 625 powder was a commercial product designed for laser cladding, characterized by a spherical shape and with a nominal particles size distribution of +150 -75 *μm*. Its composition is reported in Table 1.

Table 1. Inconel 625 powder's composition.

Product	**Chemical composition, *wt. %***						
	Ni	**Cr**	**Mo**	**Nb**	**Si**	**Fe**	**Other**
Inconel 625	65.20	21.20	8.80	3.58	0.40	< 0.10	< 2

The process parameters used for laser cladding were [12]: laser beam power = 900 *W*; scanning speed = 15 *mm/s*; powder feeding rate = 16.5 *g/min*; carrier gas flux = 4 *L/min*; protection gas flux = 14-15 *L/min*; overlap between subsequent tracks = 40%.
The obtained clads were isothermally oxidised at 800 *ºC* for different exposition times: 24, 48, 72, 168, and 336 *hours*.
The microstructure of the as treated and the oxidised clads were studied by means of a Hitachi S-3400 scanning electron microscope (SEM) equipped with an energy dispersive X-ray microanalyser (EDX). Secondary (SE) and backscattered (BSE) electron images were taken. To this scope, samples cross sections were cut, mounted, grinded with SiC papers, and finally polished in diamond slurry of up to 1 *μm* nominal size. The samples were then cleaned in deionised water, then with

propanol, and finally dried with compressed air. To enhance the microstructure visibility, the samples were electrochemically etched.

The clads' elastic modulus (E) and hardness (H) were measured by depth sensing indentation (DSI) tests performed on the polished (Ra ≈ 0.3-0.4 *μm*) plain-view surfaces of the coatings. A Nanoindenter Agilent G200, equipped with a Keysight XP indentation head with a resolution of 50 *nN* in force and < 0.01 *nm* in displacement, was used. A Berkovich indenter with an ideal tip radius of 50 *nm* was mounted to execute the indentations. The tests were executed following the instructions of the ISO 14577 standard. A continue stiffness measurement (CSM) technique was employed. The contact stiffness was continuously measured and registered during the loading phase by the imposition of a small dynamic oscillation of 2 *nm* and 45 *Hz* on the displacement signal. The amplitude and phase of the correspondence force is measured [13,14]. Continuous loading/unloading cycles were so imposed during the loading phase and applying the Oliver-Pharr methodology [15] at each unloading cycle, it is possible to obtain an evolution of the elastic modulus and hardness values along the penetration depth. 5 matrix of 5x4, for a total of 100 indentations, were programmed in each samples in 5 different zones of the polished surfaces to obtain a better average of the studied properties. A previous calibration procedure was carried out on a commercial bulk Inconel 600 sample, with a known E = 214 *GPa*, according to the CSM methodology [14]. The real contact area (A_c) of the indenter was obtained as a function of the contact depth (h_c) as proposed by Oliver and Pharr [13].
The DSI conditions were selected after previous *force control* tests. Finally, a maximum penetration depth of 1500 *nm* was fixed to affect a volume large enough to obtain average values of E and H of the studied clads. The indentations were separated of 200 *μm* to avoid interactions between them.
The hardness data were then treated to consider the indentation size effect (ISE) [16-18], and so obtain values of asymptotic hardness (H_0), using the Proportional Specimen Resistant (PSR) model proposed by Li and Bradt [19].
In addition, Vickers microhardness tests, with an applied load of 300 *gf* and an application time of 12 *s*, were performed with a Buehler 2101 microindenter

The wear behaviour of the clads was analysed in terms of local wear rate and was measured by means of local scratch tests [20], performed on the polished plain-view surfaces of the coatings, using a calibrated Berkovich tip indenter with the largest edge as leading border, as schematise in Figure 1(a).

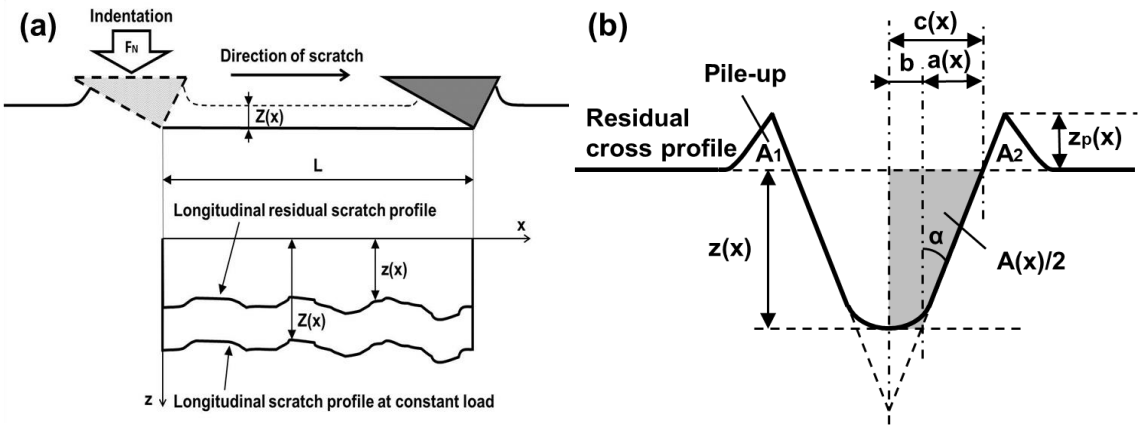

Figure 1. Scratch test scheme. (a) Longitudinal view; and (b) residual groove cross section.

A first step of evaluation of the scratch parameters was done performing local scratch tests onto the Inconel 625 as treated clad and varying the scratch normal load (F_N) and the scratch velocity (v_S) between the following listed values:

- F_N = 10 *mN*, 50 *mN*, 100 *mN*, 250 *mN*;
- v_S = 5 *μm/s*, 10 *μm/s*, 30 *μm/s*.

All the possible combinations were tested. The local wear rates calculated result did not vary significantly as a function of the F_N and the v_S in the studied ranges. No changes in the wear mechanisms were observed and finally, the combination F_N = 100 *mN*, v_S = 10 *μm/s* was selected. 3 tests were done on each one of the 5 zones of the coatings surfaces where the DSI tests were previously performed. A total of 15 scratches were so executed for each sample. The scratch length (L) was set to 300 *μm* and the tests of each zone were separated between them of 200 *μm*. A measure of the residual groove cross profile was done for each test at L/2 with the same Berkovich tip applying a load of 50 *μN*.

The local wear rate was evaluated as a function of the volume of material displaced (V_d) during the scratch test per unit of normal force and scratch length, according to equation (1), and was expressed in $mm^3N^{-1}m^{-1}$ [21,22]:

$$k = \frac{V_d}{F_N \cdot L} \tag{1}$$

where k represents the dimensional wear rate.

The volume displaced during the scratch test was calculated as a function of the longitudinal residual scratch profile (Figure 1(a)) and the groove cross profile (Figure 1(b)) as shown in equation (2):

$$V_d = \int_0^L A(x)\,dx = \int_0^L \left(z(x)^2 \cdot \tan\alpha + 2 \cdot z(x) \cdot b\right) dx \tag{2}$$

If the tip rounding became negligible, b → 0 and equation (2) could be writing as:

$$V_d = \int_0^L \left(z(x)^2 \cdot \tan\alpha\right) dx \tag{3}$$

where z is the depth of the longitudinal residual profile that is a function of the scratch distance, x, defined between 0 and L. α represents the semi-angle between the sides of the scratch groove, measured in the residual cross profile.

The scratch grooves were analysed with SEM to evaluate the wear mechanisms.

3.- RESULTS AND DISCUSSION

3.1.- Microstructure

Coatings with an average thickness of 1.65±0.16 *mm* were obtained, free of interconnected pores and cracks, and with just some punctual inter-run pore at the clad/substrate interface that did not affect the strong metallurgical bond achieved (Figure 2(a)). A homogeneous dendritic γ-Ni microstructure was observed with secondary phases segregated in the interdendritic zones (Figure 2(b)) enriched in Mo and Nb with respect to the dendrites body (Figure 2(c), and (d)) [11,12].

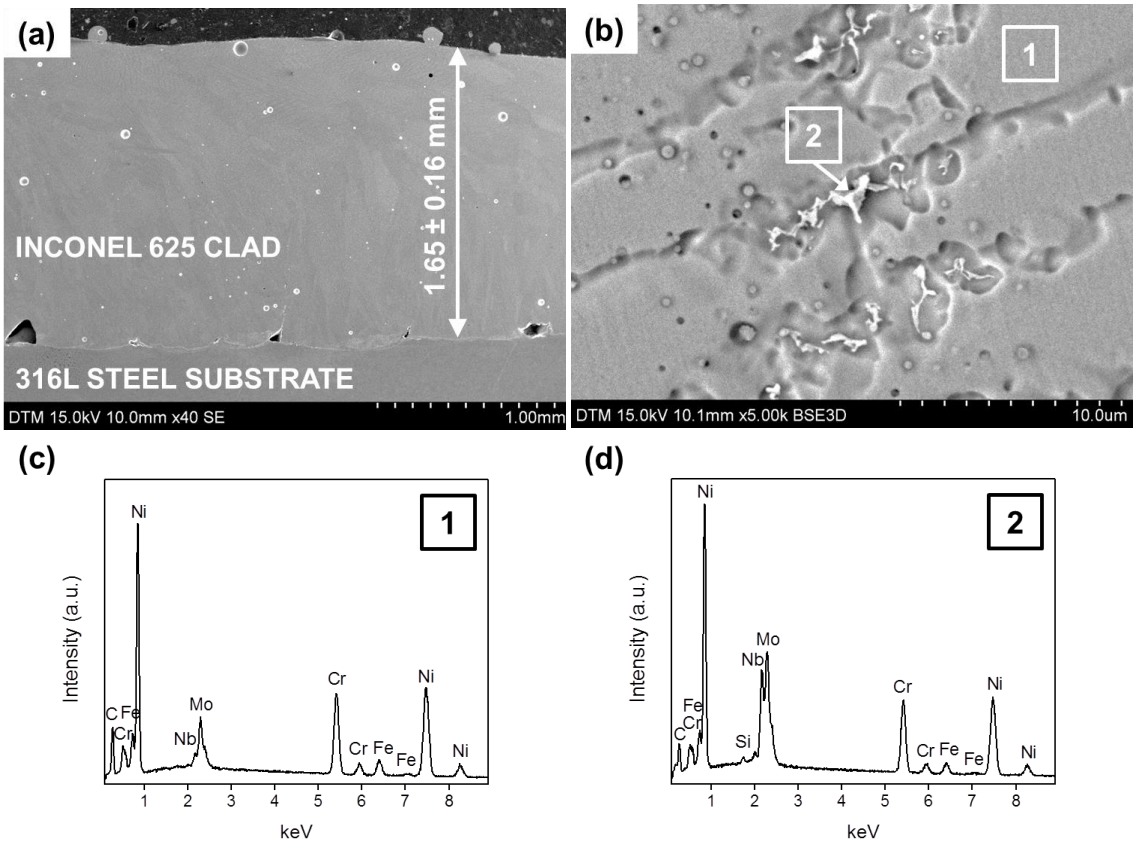

Figure 2. (a) SE image of the Inconel 625 clads cross section, and (b) BSE image of the dendritic microstructure showing interdendritic secondary phases. (c) EDX spectrum of the dendrites, mark 1 in Figure 2(b); and (d) EDX spectrum of the second phases, mark 2 in Figure 2(b).

After exposition at 800 *ºC*, the presence of irregular blocky shape Laves and needle like δ (Ni_3Nb) phases were observed at the interdendritic zones for every exposition time tested [23,24]. These secondary phases grew from the minimum tested time of 24 hours (Figure 3(a)) until the maximum one of 336 hours (Figure 3(b)), where they extend their presence also into the dendritic zones.

High contents of Mo and Nb, and presence of Si were observed in these phases. While the EDX spectrum obtained for the Laves phase (Figure 3(c)) results similar to that obtained for the secondary phases observed in the as treated clads, and reported in Figure 2(d), the δ phase shows a higher content of Nb (Figure 3(d)).

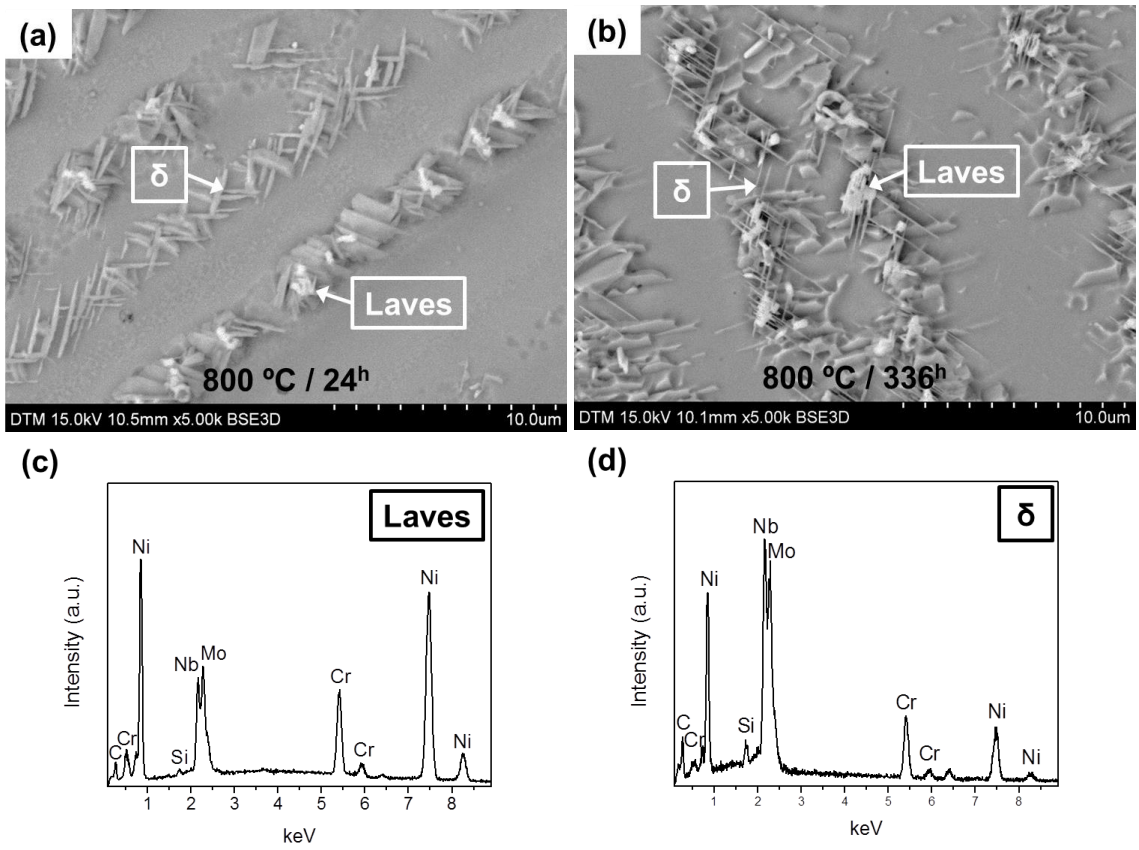

Figure 3. BSE images of the Laves and δ precipitates in the Inconel 625 clads' dendritic microstructure after exposition at 800 *ºC* for (a) 24 *hours*, and (b) 336 *hours*. (c) EDX spectrum of the Laves phase; and (d) EDX spectrum of the δ phase.

3.2.- Mechanical properties

Table 2 shows the values of E and H_0 obtained from the DSI tests. Comparing the values of the asymptotic hardness with those of the Vickers hardness tests ($HV_{0.3}$, also reported in Table 2), it is clear that the PSR model correctly analyse the ISE of the hardness measurements obtained from the DSI tests.

Both the E and the H_0 show an increase of their values with the exposition at high temperature (Figure 4). While an increase of the 17% of the E was achieved, the H_0 shows a rise of the 48% after 336 *hours* of exposition. These results agree with the microstructural changes presented by the coatings during the oxidation at 800 *ºC* that promote the growth of secondary phases with higher values of E and H_0 with respect to the Inconel 625 alloy γ-Ni structure [25,26].

Table 2. Mechanical properties of the Inconel 625 clads as treated and subjected to isothermal oxidation process at 800 *ºC* for different exposition time.

Time	**E**	**H_0**	**$HV_{0.3}$ (12s, 40x)**	**E/H0**
(*hours*)	**(*GPa*)**	**(*GPa*)**	**(*GPa*)**	**(*/*)**
0	204 ± 3	2.1 ± 0.1	2.4 ± 0.1	98.2 ± 2.6
24	218 ± 3	2.7 ± 0.1	2.8 ± 0.1	80.6 ± 1.6
48	223 ± 2	2.9 ± 0.1	3.0 ± 0.1	76.5 ± 1.7
72	238 ± 2	2.9 ± 0.1	3.1 ± 0.1	81.6 ± 1.7
168	236 ± 2	3.0 ± 0.1	3.0 ± 0.1	79.3 ± 2.0
336	238 ± 2	3.1 ± 0.1	3.3 ± 0.1	76.8 ± 1.6

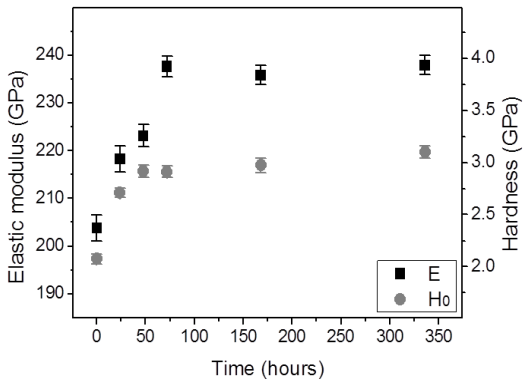

Figure 4. Elastic modulus and asymptotic hardness evolution with the oxidation time.

3.3.- Local wear behaviour

The values of k calculated by means of equation (1) are reported in Table 3. It is possible to observe a decrease of k corresponding to an improvement of the wear resistance of the clad, increasing the time of exposure at high temperature.

Table 3. Local wear behaviour of the Inconel 625 clads as treated and exposed at 800 ^{o}C.

Time (***hours***)	**k (x10^{-3})** (***mm^{3}N^{-1}m^{-1}***)	**f_{ab}** (*/*)	**ϕ (x10^{-2})** (*/*)	**k_{CUT} (x10^{-3})** (***mm^{3}N^{-1}m^{-1}***)	**k_{PD} (x10^{-3})** (***mm^{3}N^{-1}m^{-1}***)
0	13.35 ± 2.76	0.09 ± 0.05	2.8 ± 0.6	1.24 ± 0.63	12.11 ± 2.33
24	12.64 ± 2.35	0.20 ± 0.06	3.4 ± 0.6	2.55 ± 0.77	10.09 ± 1.32
48	12.14 ± 2.17	0.30 ± 0.07	3.5 ± 0.6	3.67 ± 0.84	8.47 ± 1.75
72	11.06 ± 2.91	0.23 ± 0.13	3.2 ± 0.9	2.54 ± 1.06	8.52 ± 1.57
168	12.60 ± 1.68	0.24 ± 0.07	3.8 ± 0.5	3.01 ± 0.84	9.59 ± 0.75
336	7.79 ± 1.74	0.19 ± 0.17	2.4 ± 0.6	1.49 ± 0.93	6.30 ± 1.47

The residual scratch groove left in the as treated Inconel 625 clad shows a regular shape, piling-up material on the sides of the path, and the presence of deformation bands inside and outside the scratch tracks (Figure 5(a)). These morphological characteristics suggest that the micromechanism that governs the wear behaviour in this case is mainly plastic deformation. On the other hand, the residual grooves left in the oxidised samples, shows an irregular shape, piling-up material on the sides but without presence of deformation bands (Figure 5(b)). These characteristics suggest that other micromechanisms become important.

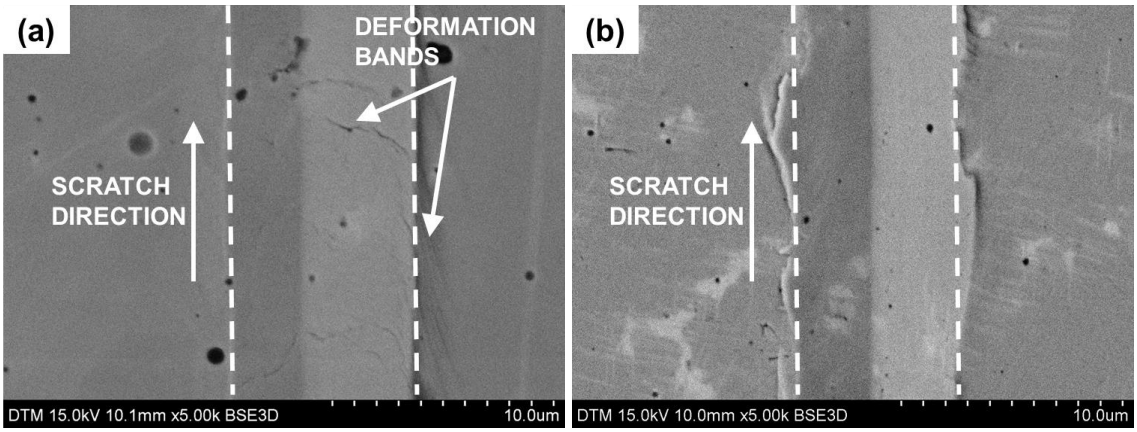

Figure 5. SE images of the scratch path in the Inconel 625 clads (a) as treated, and (b) after isothermal oxidation at 800 *ºC* for 336 *hours*.

These observations were confirmed comparing also variations of the E/H_0 ratios, reported in Table 2, with those of the k. The E/H_0 represents in fact measurements of the plastic flows, in accordance with the Greenwood and Williamson theory [27].
As the differences in the E/H_0 ratios differ from those of the k at the different exposition time, and thanks to the microstructural considerations previously done on the residual groove, it was deduced that the plastic deformation was not the only micromechanisms responsible of the wear behaviour of the clads after isothermal high temperature oxidation (Figure 6).

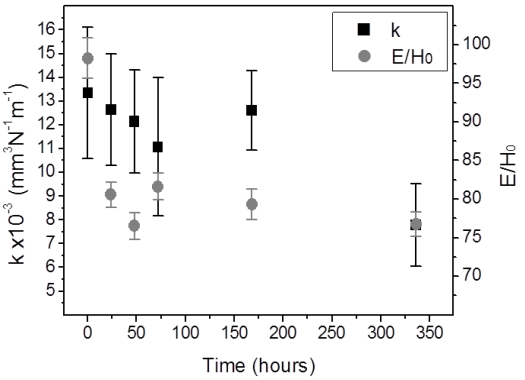

Figure 6. Dimensional wear rate (k) and E/H_0 ratio evolutions as a function of the oxidation time.

Four type of wear micromechanisms have been defined: microcutting, microploughing, microfatigue, and microcracking [21,28]. As the scratch tests performed in this work were characterized by a single pass and no cracks were detached in the residual groove, no effects of microfatigue and microcracking were generated. To evaluate the percentage of microcutting, Zum Gahr [28] suggested measuring the volume of removed material that was transformed in wear particles, by means of a parameter f_{ab}, function of the geometrical characteristics of the residual groove cross section (Figure 1(b)). It was defined as $f_{ab} = 1-(A_1+A_2)/A$ and results equal to 1 when only microcutting were generated (no pile-up on the groove sides). Working out the Rabinowicz theory [21], it is possible to define a dimensional wear rate of microcutting as $k_{CUT} = \phi \cdot f_{ab}/H_0$, where ϕ represent a geometrical factor that depends on the depth of the longitudinal residual profile z(x) and the semi-angle between the sides of the scratch groove, α. A dimensional wear rate of microploughing could be so calculated as $k_{PD} = k-k_{CUT}$.

The values of f_{ab}, ϕ, k_{CUT}, and k_{PD} for the different samples, were reported in Table 3. When the harder Laves and δ precipitates grew in the Inconel 625 clads, during exposition at high temperature, the plastic deformation of the alloy is restricted, as the decrease of the E/H_0 ratio indicates [27]. A reduction of the microploughing mechanism was experimented (Figure 7(a)). An improvement of the wear resistance of the coating was measured. By the way, the presence of an additional microcutting mechanism, that became important especially for the lower time of exposition at high temperature (Figure 7(b)), results in higher values of the k and a lower improvement of the wear behavior with respect to those obtained if only microploughing was presented.

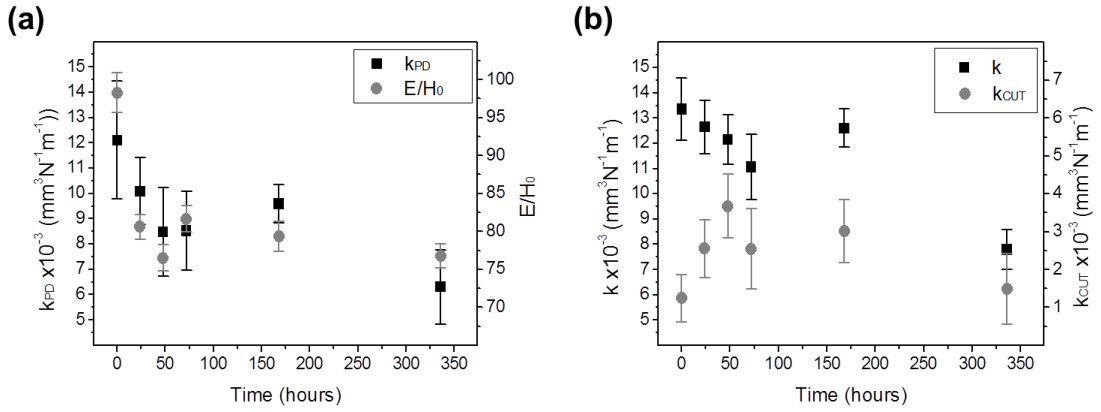

Figure 7. (a) Dimensional wear rate of microploughing (k_{PD}) and E/H_0 ratio evolutions, and (b) dimensional wear rate (k) and dimensional wear rate of microcutting (k_{CUT}) evolutions, as a function of the oxidation time.

4.- CONCLUSIONS

The local wear behaviour of Inconel 625 coatings obtained by laser cladding and exposed to isothermal high temperature oxidation at 800 *ºC* were studied by means of depth sensing indentation and local scratch tests. The micromechanisms responsible of the wear behaviour were identified and correlated with the microstructural changes that occur into the clad. The following conclusions can be drawn:

- After exposition at 800 *ºC*, the interdendritic zones of the clad were characterized by the presence of Laves and δ phases.
- Depth sensing indentation tests permit to identify the growth of the elastic modulus and the hardness of the coatings with the time of exposure at high temperature corresponding to the generation of Laves and δ hardening phases.
- The wear behaviour of the as treated Inconel 625 clads is dominated by plastic deformation (microploughing).
- The growth of the Laves and δ phases reduce the ductility of the alloy and increase the wear resistance of the Inconel 625 clads. At the same time, the fragile behaviour of these particles, introduces an additional mechanism of wear by microcutting.

ACKNOWLEDGEMENTS

The authors would like to thank the Spanish government CICYT through grants MAT2010-18916 and MAT2013-41784-R, the Universidad Rey Juan Carlos project URJC-CM-2010-CET-5550 and the European Union Seventh Framework

Programme (FP7/2007-2013) under grant agreement number 605207 for financial support.

REFERENCES

[1] H.L. Elselstein and D.J. Tillack. The invention and definition of Alloy 625. Paper presented at International Symposium on Superalloys 718, 625 and Various Derivatives, Pittsburgh, (1991) 1-14.

[2] C.P. Paul, P. Ganesh, S.K. Mishra, P. Bhargava, J. Negi, A.K. Nath. Investigating laser rapid manufacturing for Inconel-625 components. Optics & Laser Technology, 39 (2007) 800-805.

[3] J. Adamiec. High temperature corrosion of power boiler components cladded with nickel alloys. Materials Characterization, 60 (2009) 1093-1099.

[4] G.P. Dinda, A.K. Dasgupta, J. Mazumder. Laser aided direct metal deposition of Inconel 625 superalloy: Microstructural evolution and thermal stability. Materials Science and Engineering A, 509 (2009) 98-104.

[5] Ashby, M.F. and Jones, D.R.H., Engineering Materials 1. An Introduction to their Properties and Applications, 2nd Ed. Butterworth-Heinemann, Oxford, UK, 2002.

[6] Grainger, S. and Blunt, J., Engineering Coatings. Design and Application. Abington Publishing, Cambridge, UK, 1998.

[7] T. Baldridge, G. Poling, E. Foroozmehr, R. Kovacevic, T. Metz, and V. Kadekar. Laser cladding of Inconel 690 on Inconel 600 superalloy for corrosion protection in nuclear applications. Optics and Lasers in Engineering, 51 (2013) 180-184.

[8] J. de Damborenea, A.J. Vázquez, B. Fernández. Laser-clad 316 stainless steel with Ni–Cr powder mixtures. Materials and Design, 15 (1994) 41-44.

[9] Farson, D.F., Ready, J.F., Feeley, T., Handbook of Laser Materials Processing. Orlando: Laser Institute of America; 2001.

[10] Toyserkani, E., Khajepour, A., Corbin, S., Laser-Cladding. Florida: CRC Press LLC; 2005.

[11] D. Verdi, M.A. Garrido, C.J. Múnez, P. Poza. Cr_3C_2 incorporation into an Inconel 625 laser cladded coating: Effects on matrix microstructure, mechanical properties and local scratch resistance. Materials and Design, 67 (2015) 20-27.

[12] D. Verdi, M.A. Garrido, C.J. Múnez, P. Poza. Mechanical properties of Inconel 625 laser cladded coatings: Depth sensing indentation analysis. Materials Science and Engineering A, 598 (2014) 15-21.

[13] W.C. Oliver and G.M. Pharr. Measurement of hardness and elastic modulus by instrumented indentation: Advances in understanding and refinements to methodology. Journal of Materials Research, 19 (2004) 3-20.

[14] X. Li and B. Bhushan. A review of nanoindentation continuous stiffness measurement technique and its applications. Materials Characterization, 48 (2002) 11-36.

[15] W.C. Oliver and G.M. Pharr. An improved technique for determining hardness and elastic modulus using load and displacement sensing indentation experiments. Journal of Materials Research, 7 (1992) 1564-1583.

[16] Fischer-Cripps, A.C., Nanoindentation, 3rd Ed. Springer, New York, USA, 2011.

[17] W.D. Nix and H. Gao. Indentation size effects in crystalline materials: a law for strain gradient plasticity. Journal of the Mechanics and Physics of Solids, 46-3 (1998) 411-425.

[18] Y. Huang, F. Zhang, K.C. Hwang, W.D. Nix, G.M. Pharr, G. Feng. A model of size effects in nano-indentation. Journal of the Mechanics and Physics of Solids, 54 (2006) 1668-1686.

[19] H. Li and R.C. Bradt. The microhardness indentation load/size effect in rutile and cassiterite single crystals. Journal of Materials Science, 28 (1993) 917-926.

[20] S.P. Wen, R.L. Zong, F. Zeng, Y. Gao, F. Pan, Investigation of the wear behaviours of Ag/Cu multilayers by nanoscratch, Wear 265 (2008) 1808-1813.

[21] Rabinowicz, E., Friction and wear of materials. 2nd Ed. John Wiley & Sons, Inc., USA, 1995.

[22] J.F. Archard. Contact and rubbing of flat surfaces. Journal of Applied Physics, 24 (1953) 981-988.

[23] S. Floreen, G.E. Fuchs, W.J. Yang. The metallurgy of Alloy 625. Superalloys 718, 625, 706 and Various Derivatives (1994) 13-37.

[24] Davis, J.R., *ASM Speciality Handbook: Nickel, Cobalt and Their Alloys*. ASM International, USA, 2000.

[25] S. Dai, W. Liu. First-principles study on the structural, mechanical and electronic properties of δ and γ'' phases in Inconel 718. Computational Materials Science 49 (2010) 414-418.

[26] Y. Cao, J. Zhu, Z. Nong, X. Yang, Y. Liu, Z. Lai. First-principles studies of the structural, elastic, electronic and thermal properties of Ni_3Nb. Computational Materials Science 77 (2013) 208-213.

[27] J.A. Greenwood and J.B.P. Williamson. Contact of nominally flat rough surfaces, Proceedings of the Royal Society of London A 295 (1966) 300-319.

[28] K.H. Zum Gahr. Modelling of two-body abrasive wear. Wear 124 (1988) 87-103.